THE JOURNAL OF PHYSICAL CHEMISTRY B
A JOURNAL OF THE AMERICAN CHEMICAL SOCIETY

pubs.acs.org/JPCB

Article

Viscoelasticity and Noise Properties Reveal the Formation of Biomemory in Cells

Evangelos Bakalis,* Vassilios Gavriil, Alkiviadis-Constantinos Cefalas, Zoe Kollia, Francesco Zerbetto, and Evangelia Sarantopoulou

Cite This: *J. Phys. Chem. B* 2021, 125, 10883−10892

Read Online

ACCESS | Metrics & More | Article Recommendations | Supporting Information

ABSTRACT: Living cells are neither perfectly elastic nor liquid and return a viscoelastic response to external stimuli. Nanoindentation provides force−distance curves, allowing the investigation of cell mechanical properties, and yet, these curves can differ from point to point on the cell surface, revealing its inhomogeneous character. In the present work, we propose a mathematical method to estimate both viscoelastic and noise properties of cells as these are depicted on the values of the scaling exponents of relaxation function and power spectral density, respectively. The method uses as input the time derivative of the response force in a nanoindentation experiment. Generalized moments method and/or rescaled range analysis is used to study the resulting time series depending on their nonstationary or stationary nature. We conducted experiments in living *Ulocladium chartarum* spores. We found that spores in the approaching phase present a viscoelastic behavior with the corresponding scaling exponent in the range 0.25−0.52 and in the retracting phase present a liquid-like behavior with exponents in the range 0.67−0.85. This substantial difference of the scaling exponents in the two phases suggests the formation of biomemory as a response of the spores to the indenting AFM mechanical stimulus. The retracting phase may be described as a process driven by bluish noises, while the approaching one is driven by persistent noise.

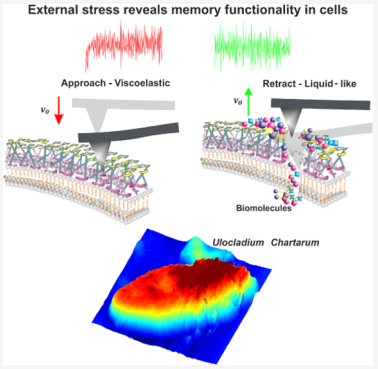

INTRODUCTION

Living cells are continuously subject to mechanical forces both by surrounding cells and by the microenvironment they belong to. They adapt their bioresponse to extracellular environmental conditions by tracing maximum viability lines.[1,2] On a single cell, mechanical forces may cause shear, stress, and torsion. The generally accepted scenario is that in a cell, the response to mechanical deformations is due to the activation of external cell wall protein-like mechanosensors, which are connected internally with an extended plasma membrane contractile network formed mainly by actin filaments.[3−6] Response to external stimuli determines the elastic properties of a cell surface and relates them to concrete tasks, for example, softening supports cell mobility and migration.[3] Cell elasticity is a measure whose changes are used as indicators for cytotoxicity, malignancy, viability, biomemory, and abnormalities.[1−9] Furthermore, changes of cell elasticity, resulting from external stress, have been associated with cell abnormalities such as cancer, cardiomyopathies, and generation of diverse dysmorphic phenotypes.[8,10,11] This property has been used for on-the-fly cell mechanical phenotyping.[12] Cell mechanics, which examines the response of a cell to the stimuli of biochemical, chemical, or physical nature,[13,14] has been investigated by applying different techniques, including atomic force microscopy nanoindentation (AFM-NI); see a recent comparison of methods to assess cell mechanical properties.[15]

AFM-NI has been widely used to characterize the mechanical properties of both cells and tissues.[13,16,17] It uses a tip of well-defined geometry to punch into the cell placed on a solid support and is commonly used to quantify mechanical properties at a subcellular resolution. It can also perform precise force measurements at desired cellular locations where the tip of the cantilever is used as the indenter. The measured force, attractive or repulsive, corresponds to the interaction between tip atoms and those that belong to the sample surface. The vertical displacement of a cantilever and its deflection are recorded simultaneously and then converted into force−distance curves (FDCs). FDCs are registered in both phases: approach (tip moving toward the sample) and retraction (tip withdrawing from the sample).

To a first approximation, Young's modulus is estimated by using the Hertz model,[18,19] which describes the response of an isotropic and fully elastic material under a load, to fit the FDCs. In this approximation, Young's modulus is time-independent. For complex materials such as cells, the estimate

Received: February 26, 2021
Revised: September 6, 2021
Published: September 21, 2021

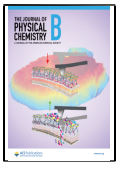

https://doi.org/10.1021/acs.jpcb.1c01752
J. Phys. Chem. B 2021, 125, 10883−10892

of Young's modulus based solely on the Hertz model and without considering viscoelastic effects (combination of elastic and liquid behavior) is highly questionable. Young's modulus is a time-dependent measure, and its estimate is affected both by the thickness of the cell and by the solid support where it is placed on.[20,21] Experimentally, the nonidentical approach and retraction parts of FDCs are signs of viscoelasticity. A reason for the differences likely is the diverse hydrodynamic drag on the cantilever. Furthermore, in the contact regime, a difference between approach and retraction is an indication of plastic deformations or, most typically, a viscoelastic behavior of the sample, which underlines the formation of a type of memory (biomemory) because the cell alters its local environment via excessive protein activity at the activation site.[2]

Cells are not a simple fluid-filled envelope; they contain different active intracellular structures that may display distinct mechanical properties.[14] Cells display both solid-like elastic and fluid-like viscous properties and typically return a viscoelastic behavior under external stress, which is reflected on a power-law form satisfied by both the creep and the stress relaxation functions.[22,23] A vast number of studies based on a variety of techniques showed that the rheological properties of cells are better described by a power-law relaxation function of the form $E(t) = E_0(t/t_0)^{-\beta}$ with $0 \leq \beta \leq 1$. E_0 is Young's modulus at time t_0, which can be chosen arbitrarily and is usually set to 1 s.[24] E_0 deviates from Young's moduli provided by elastic models which are constant in time. The scaling exponent β characterizes the degree of fluidity and energy dissipation upon deformation. A value of $\beta = 0$ stands for a perfectly elastic solid and a value of $\beta = 1$ for a Newtonian liquid. Any value of the scaling exponent between these two limits describes a viscoelastic medium. A typical value of β for cells lies in the range 0.1−0.3, thus classifying a cell as a viscoelastic solid.[24−27] For cells, it has been reported that the dependency of the elastic modulus on probing frequency follows a weak power law, which resulted in the absence of discrete relaxation times in the system.[28] For viscoelastic materials, such as cells, their response is not only a function of the instantaneous deformations caused by the exerted mechanical forces but also depends on the history of deformations.[29,30]

In specific fungal and carcinogenic cells, an external stress is always followed by a bioresponse for maximum viability via a biomemory cell system.[1,2,8,9] A memory kernel can describe the history of deformations, and its form indicates how strong is the memory formed under the action of mechanical forces. For example, a Dirac delta memory kernel describes memoryless deformations, an exponential decay can describe a Poisson distribution of deformations, and a power-law memory kernel accounts for strong memory effects. History-dependent deformations in viscoelastic systems, where elastic and viscous properties coexist to varying degrees, may cause nonlocal effects in both time and space[31] and may be modeled by fractional calculus,[32] which is an appropriate framework to model complexity.[33,34] Additionally, complexity may be modeled by a fractional Langevin equation where the overall noise may behave as a multiplicative process. The role of such a class of noises has been studied for a variety of systems ranging from ecology[35] to pattern formation[36] and to the stability of biological systems.[37] Experimentally, the complexity of the mechanical behaviors to deformations in single cells and/or tissues has been pointed out;[30,38−41] see also a recent review.[42]

Considering a cell as an incompressible material, its response to a mechanical load may be expressed as a function of the indentation depth and the creep relaxation function through their convolution.[42] In an AFM-NI experiment, the response forces form a data set with a hierarchical time distribution and define the observation window. The analysis of events in such a window, which usually contains few data points, can infer past and future events only if the process is deterministic or periodic or stationary. For nonstationary processes, such as approach and retraction parts of a FDC, one can use more sophisticated methods, appropriate for time series analysis. Among them,[43−48] the generalized moments method (GMM) is generally one of the more robust and works well even for short time series.[49] It has been successfully applied in numerous fields,[50−55] and it works for nonstationary time series.[54,55] For the stationary ones, rescaled range analysis (RA)[56,57] or some variations thereof[58] are the proper analysis methods. Both methods, GMM and RA, deliver the scaling exponent, which is called the Hurst exponent, of a stochastic process. Additionally, there is a link between these scaling exponents and the scaling of the power spectral density (PSD) whose value classifies the color of the stochastic process.[59] To distinguish the method applied for analysis, the symbols with subscripts H_{GMM} and H_{RA} are used. If one treats a time series with GMM and the latter returns a zero value for H_{GMM}, it means that the time series is stationary and its analysis should be made either by rescaled RA or any other method proper for the analysis of stationary time series. Instead, if a time series is analyzed by RA and the latter returns a Hurst exponent higher than one, then it is not stationary and analysis should be made by GMM.

In the present work, viscoelastic and noise analyses of the approaching−retracting AFM-NI responses of *Ulocladium chartarum* spores suggest the presence of the biomemory effect in the cell functionality during external forcing, in agreement with previous works.[1,2] We define the response force, for the pyramidal tip, for both approach and retraction parts of a FDC, and we extend the analysis in order to obtain in a single run both the viscoelastic scaling exponent and the scaling exponent of the PSD that underlines the type of the environmental noise. The latter can operate as a starting input in advanced mathematical modeling and fractional calculus, where knowledge of the environment's noisy properties is mandatory.

Power-Law Rheology and FDCs under the Linear Ramp. The response force, $f(h)$, consists of the recorded values of the deflection signal with $h(t)$ being the indentation depth. Assuming that a rigid indenter goes against and/or penetrates a linear viscoelastic sample, $f(t)$ and $h(t)$ are related through convolution integrals, first introduced for spherical indenters[60]

$$f_n(t) = \bar{C}_n \int_0^t E(t - t') \frac{\partial h^n(t')}{\partial t'} \, dt' \tag{1}$$

and

$$h^n(t) = C_n \int_0^t J(t - t') \frac{\partial f(t')}{\partial t'} \, dt' \tag{2}$$

where $\bar{C}_n = {C_n}^{-1}$ and the index n stands for the type of the indenter, with $n = 1$ for a flat-ended cylindrical indenter with radius R, $(C_1 = 1 - \nu/R)$,[61] $n = 3/2$ for a spherical indenter, $(C_{3/2} = 3(1 - \nu^2)/4R)$,[18] and $n = 2$ either for a conical

https://doi.org/10.1021/acs.jpcb.1c01752
J. Phys. Chem. B 2021, 125, 10883−10892

indenter, ($C_{2,con} = \pi(1 - \nu^2)/2 \tan\alpha$),[62] or for a four-sided pyramidal indenter with ($C_{2,pyr} = 1.342(1 - \nu^2)/\tan\alpha$).[63] Poisson's ratio is represented by ν and for incompressible materials takes the value of 0.5, and α is the average contact angle. $E(t)$ and $J(t)$ are the time-dependent relaxation and creep function, respectively. By taking the in-time-domain Laplace transform, $f(s) = L\{f(t)\} = \int_0^\infty f(t)\, e^{-st}$, of each one of eqs 1 and 2 and by setting $h(0) = \dot{f}(0) = 0$, one can easily see that $E(s)J(s) = 1/s^2$. Creep and relaxation functions for viscoelastic materials follow a power-law behavior, that is, $J(t) = J_0(t/t_0)^\beta$ and $E(t) = E_0(t/t_0)^{-\beta}$. E_0 and J_0 satisfy the relation $E_0J_0 = 1/\Gamma(1 - \beta)\Gamma(1 + \beta)$, with $\Gamma(z) = \int_0^\infty x^{z-1}\, e^{-x}\, dx$ being the gamma function; notice that E_0 is expressed in units of pressure (N/m^2). Equations 1 and 2 hold when the contact area is an increasing function of time.[60]

Approaching Phase. The indentation depth for constant velocity, v_0, is a linear function of time and reads $h(t) = v_0t$, for $0 < t \le t_m$ (loading or approaching phase), and $h(t) = v_0(2t_m - t)$, for $t_m < t \le 2t_m$ (unloading or retracting phase). t_m is the time needed for the tip to reach its maximum penetration depth, where the phase changes from approach to retract. At this point, the direction of the velocity changes, but its speed is kept constant. For a typical AFM FDC of 1024 sampling points, t_m corresponds to 512 sampling points and is converted into time units when multiplied by the minimum lag time, which is defined by the resolution of the machine. For a fixed number of data points and for pretty much constant maximum penetration depth, the surface anaglyph can lead to re-adjusting the initial position of the piezo, see Figure 1.

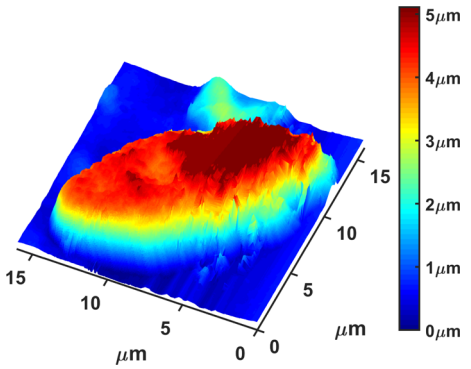

Figure 1. AFM image of an *Ulocladium chartarum* single spore recorded under standard environmental conditions. Its surface is characterized by an intense changing landscape against which the tip is moving with constant velocity v_0 (toward/away).

For $h(t) = v_0t$ and by using eq 1, one ends up with the recorded force, which reads

$$f_n(t) = \bar{C}_n E_0 v_0^n \frac{n\Gamma(1 - \beta)\Gamma(n)}{\Gamma(1 - \beta + n)}\left(\frac{t}{t_0}\right)^{-\beta} t^n \tag{3}$$

For a pyramidal type of indenter, $n = 2$, eq 3 reads

$$f_{app}(t) = \frac{2E_0v_0^2t_0^2}{C_{2,pyr}}\frac{\Gamma(1 - \beta)}{\Gamma(3 - \beta)}\left(\frac{t}{t_0}\right)^{2-\beta} \tag{4}$$

where $C_{2,pyr} = 3.2$ since we assume $\alpha = 17.5°$ (the average contact angle) and $\nu = 0.5$ (incompressible material).

Retracting Phase. Equation 4 holds for $0 < t \le t_m$ (approach) where the contact area monotonically increases as a function of time.[60] Equation 4 can also be used for retraction, when the contact area decreases, under proper modification of time by following Ting's method.[64,65] The method assumes that there exists a time moment t^*, $t^* \in (0, t_m)$, such that the contact area in the approaching phase is the same as the contact area in the retracting phase, $t \in (t_m, 2t_m)$. Therefore, the force can be obtained by eq 1 where we replace the upper limit of the integral from t to $t^*(t)$, and then, the link between the two time moments can be established by solving the following integral equation[64]

$$\int_{t^*}^{t_m} E_0\left(\frac{t - \tau}{t_0}\right)^{-\beta}\frac{dh_{app}(\tau)}{d\tau} + \int_{t_m}^{t} E_0\left(\frac{t - \tau}{t_0}\right)^{-\beta}\frac{dh_{ret}(\tau)}{d\tau} = 0 \tag{5}$$

By replacing $h_{app}(t) = v_0t$ and $h_{ret}(t) = v_0(2t_m - t)$ in eq 5 and by carrying out the integrals, we find that $t^* = t - 2^{1/1-\beta}(t - t_m)$.[21] Notice that the value of t^* depends only on the loading conditions and neither on the geometry of the tip nor on the thickness of the sample. The response force in the retracting phase is given by eq 4 where we use t^* instead of t and reads

$$f_{ret}(t) = \frac{2E_0v_0^2t_0^2}{C_{2,pyr}}\frac{\Gamma(1 - \beta)}{\Gamma(3 - \beta)}\left(\frac{t}{t_0}\right)^{2-\beta} (1 - 2^{1/1-\beta}(1 - t_m/t))^{2-\beta} \tag{6}$$

for $t \in (t_m, 2t_m)$. The time derivative of eqs 4 and 6 scales approximately as

$$\frac{\partial f}{\partial t} \approx t^{1-\beta} \tag{7}$$

Corrections in eqs 4 and 6 should be introduced to consider the influence of a solid support on the measured values of the response force. Such corrections are needed when cells, and in general samples that are measured, adhere on a surface (the solid support), usually glass whose Young's modulus is orders of magnitude higher than that of cells. Back scattering effects originated from the solid support give a significant contribution to the force, especially when the tip radius is comparable to the sample thickness.[21,42,66]

Treatment of FDCs as Time Series. FDCs, experimentally recorded, can be considered as a sequence of values of either force, $F(n)$, or distance, $h(n)$, at hierarchically distributed time moments, t_n, $n = 1, 2, 3, ..., N$ with N as the maximum number of data points. Response forces are in the range of pN to μN and are affected by environmental random forces that provide a stochastic contribution to the overall system. On the one hand, such random forces contain information about the environment and, on the other hand, likely render questionable Young's modulus values when they are the result of a direct fit of FDCs to either eq 4 or 6, vide infra.

Generalized Moments Method. A stochastic process can be memoryless, persistent, and antipersistent, where the characterization stands with respect to the kind of memory maintained by the process. If every new value of the stochastic sequence does not pose any dependence on its previous values, then we call the process memoryless. Instead, if every new value depends on its previous values, then the process possesses memory. It is called persistent when every new

https://doi.org/10.1021/acs.jpcb.1c01752
J. Phys. Chem. B 2021, 125, 10883−10892

value likely follows the previous ones' trend and antipersistent otherwise.

GMM is used to analyze nonstationary time series,[55] it is one of the most robust methods and works well even for short time series,[49] and it has been successfully applied in several diverse fields.[50−54,67] GMM uses the scaling of statistical moments of various orders including fractional ones. Briefly, GMM works as follows: It considers a time series of the form $\{x_n\}$ with $n = 1, 2, ..., N$, where N is the total number of steps (measurements). If the minimum lag time is τ—the reciprocal of the sampling frequency—then the total length of the trajectory (time) is $T = N\tau$. If $\{x_n\}$ is a self-similar process, then we expect that the time series, when zoomed in or zoomed out, will reveal the same patterns scaled by a certain amount, $\{x_{an}\} \stackrel{d}{=} \{a^H x_n\}$, where $\{..\} \stackrel{d}{=} \{..\}$ stands for the equality of finite dimensional distributions, and $H \in (0, 1)$ is the scaling exponent also known as the Hurst exponent.[56] We take the norm of the difference of $\{x_n\}$ at two distinct time moments, t and s with $(t > s)$, and we write $\|x_t - x_s\| = \|x_1\|\|t^H - s^H\|$. Furthermore, we consider three points x_t, x_s, and x_{t-s}, and their norms satisfy the inequality $\|x_t - x_s\| \leq \|x_{t-s}\| + \|x_t - x_s - x_{t-s}\|$, and by using $\|x_t\| = \|x_1\|\|t^H\|$, we then end up with $\|t^H - s^H\| \leq \|t - s\|H + \|t^H - s^H - (t - s)^H\|$, where the second term of the inequality goes as s^H for $s \ll$. In this limit, one can write $\|x(t) - x(s)\| \sim |t - s|^H$, which for various moments of order, q, reads $\|x(t) - x(s)\|^q \sim |t - s|^{qH}$. The latter has been extended to include the dependence of the Hurst exponent on the order of the moment, $H(q)$ instead of H,[33,45,68,69] since the various moments may not scale precisely by the same factor. The new exponent $z(q) = qH(q)$ is called the structure function. For discrete data sets, the time difference $t - s$ corresponds to a sliding window of length Δ, which must be small with respect to the total length of the time series.

First step: we construct the time series characterized by different lag times, Δ, which contain the absolute change of the values between two points of the initial time series, let us say $x(n)$, that are apart by Δ

$$y_n(\Delta) = \|x(n + \Delta) - x(n)\| \tag{8}$$

for $n = 1, 2, ..., (T - \Delta)/\tau$ and for $\Delta = \tau, 2\tau, ..., N/10\tau$. In order to have statistically reliable results, we define the maximum lag time as 1/10 of the maximum length of the original time series, $\tau_{max} = N/10$, thus creating $N/10$ new time series of length $(T - \Delta)$ each.

Second step: We estimate the statistical moments of $y_n(\Delta)$ according to

$$m(q, \Delta) = \frac{1}{T - \Delta} \sum_{n=1}^{T-\Delta} y_n(\Delta)^q \tag{9}$$

where fractional values of the moment, q, are also taken into account. We use only positive values of the moments.[70] Moments in the range $0 < q \leq 2$ are responsible for the core of the probability density function (PDF), while moments higher than 2, $q > 2$, contribute to the tails of the PDF.[71]

Third step: we expect that the moments scale according to the elapsed time, Δ, as a power law

$$m(q, \Delta) \approx \Delta^{z(q)} \tag{10}$$

where $z(q)$ is the structure function whose shape gives information on the stochastic mechanism(s) governing the motion. If the structure function is linear with respect to the order of the moment

$$z(q) = qH_{GMM} \tag{11}$$

then the process is monofractal, while if the structure function has a convex shape, then the process is multifractal, see for details.[54,55] Note that in eq 11, H has been replaced by H_{GMM} to distinguish the analysis method.

Rescaled Analysis. Let us assume that f_i is a stationary time series, with $i = 1, 2, 3, ..., N$. We divide the time series into L nonoverlapping windows (subperiods) of length Δ, $L = \lfloor N/\Delta \rfloor$. Δ provides the number of data points in a given subperiod that should be small with respect to N and takes on the role of time when multiplied by the time lag. We fix its maximum value to $\Delta_{max} = \lfloor N/4 \rfloor$, while its minimum value is set to $\Delta_{min} = 10$. The number of the nonoverlapping windows lies in the range $\lfloor N/\Delta_{max} \rfloor \leq L \leq \lfloor N/\Delta_{min} \rfloor$. For each one of these windows, we estimate the mean, $<f_m>_\Delta = 1/\Delta \sum_{j=1}^{\Delta} f_{(m-1)\Delta+j}$, where $m = 1, 2, ..., L$, and the standard deviation $S_m(\Delta) = \{1/\Delta \sum_{j=1}^{\Delta} (f_{(m-1)\Delta+j} - <f_m>_\Delta)^2\}^{1/2}$. We create the profile $Y_m(t) = \sum_{j=1}^{t} (f_{(m-1)\Delta+j} - <f_m>_\Delta)$. We estimate the distance $R_m(\Delta) = \max_{1 \leq t \leq \Delta}\{Y_m(t)\} - \min_{1 \leq t \leq \Delta}\{Y_m(t)\}$. We average all over the L-windows, $S(\Delta) = 1/L \sum_{m=1}^{L} S_m(\Delta)$, and $R(\Delta) = 1/L \sum_{m=1}^{L} R_m(\Delta)$, and we define the rescaled range (R/S) (Δ) which scales as[72]

$$\left(\frac{R}{S}\right)(\Delta) = \frac{1}{S_\Delta}\{\max_{1 \leq t \leq \Delta}\{Y(t)\} - \min_{1 \leq t \leq \Delta}\{Y(t)\}\} \sim \Delta^{H_{RA}} \tag{12}$$

The quantity $(R/S)(\Delta)$ returns the rescaled distance between the maximum and minimum values of the time series of a given window of length Δ. According to the scaling described by eq 12, this quantity is a monotonically increasing function of the length of the window. If in this description f_i represents the differentiation of the response force recorded in AFM-NI, then the scaling described by eq 12 is the discrete analogue of the scaling described by eq 7. This is true because the time derivative of the response force (approach or retract), eq 7, is a monotonically increasing function of time for $0 < \beta < 1$.

Linear regression of eq 12 provides the exponent H_{RA}

$$\ln\left(\frac{R}{S}\right)(\Delta) = A + H_{RA} \ln(\Delta) \tag{13}$$

By equating the exponent of eq 7 with the scaling exponent predicted by RA, eq 13, we end up with

$$H_{RA} = 1 - \beta \tag{14}$$

Equation 14 allows estimating the scaling exponent β whose value classifies the cell as elastic or liquid or viscoelastic.

For the construction of the time series f_i from the recorded FDC data, we work as follows. In the approaching phase, the values F_0^{app} and F_1^{app} correspond to the response signal to the left of and at the contact point (CP), and the value F_N^{app} corresponds to the response force at $t = t_m$. In the retracting phase, F_0^{ret} and F_1^{ret} correspond to the values of the response force at $t = t_m$ and $t = t_m + \tau$, respectively, and F_N^{ret} gives the value at the CP. A two-step preprocessing is required for further analysis; first, we define the time series $\phi_i^j = F_i^j - F_0^j$, $i = 0, 1, 2, ..., N$, which describes the raw data shifted by the initial value, (F_0^j), and second, we differentiate the sequences with respect to time, $f_i^j = \phi_i^j - \phi_{i-1}^j$, with $i = 1, 2, ..., N$. The

https://doi.org/10.1021/acs.jpcb.1c01752
J. Phys. Chem. B 2021, 125, 10883−10892

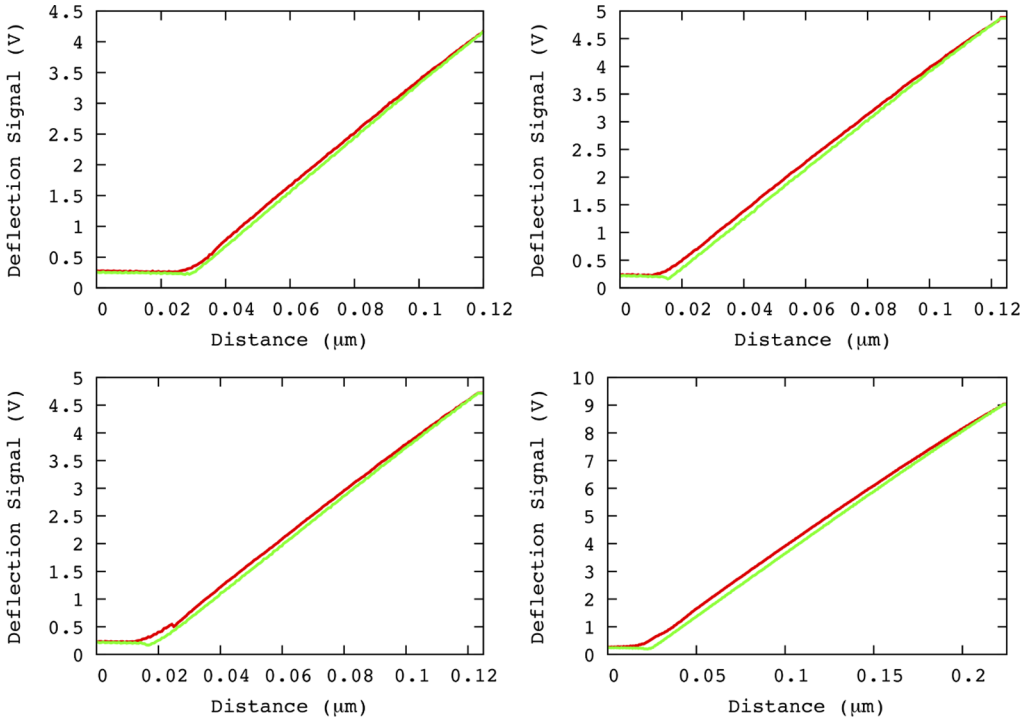

Figure 2. Color code: red for approach and green for retraction. A part of FDCs for some typical experiments analyzed in this study are depicted.

new time series, f_i^j, is the derivative of the response force multiplied by τ. On the other hand, the accumulation of f_i^j up to a certain time moment gives the shifted response signal, $\phi_m^j = \sum_{i=1}^{m} f_i^j$. For f_i^j being stationary, RA is used and the viscoelastic exponent is provided by eq 14. For nonstationary f_i^j, GMM is used and the viscoelastic exponent is again provided by eq 14 where we replace H_{RA} with H_{GMM}.

Parallel to the environmental noise, an instrumental AFM noise, which is a function of instrumental, thermal, acoustic, electronic and quantum noises, and so forth, is also present. These additional noise contributions are characterized by different time scales and probably die out at the time scale defined by the resolution of the instrument. Constant contributions arising from an AFM noise cannot affect our analysis because the proposed methodology is based on differences between values of subsequent steps that cancel out constant contributions. If, however, these components of AFM noise are not constant in time and turn the measured signals (their time derivatives) into multiplicative ones (i.e., nonstationary), then their nature can be identified by the GMM, which returns a structure function of convex shape, vide infra.

Power Spectral Density. A widely accepted measure for the classification of stationary time series is its PSD, while for nonstationary time series, this measure is questionable.[73] In many phenomena, PSD scales as

$$\mathrm{PSD}(z) \approx \frac{1}{z^{\gamma}} \tag{15}$$

where z is the variable in the frequency domain and γ is the scaling exponent whose value defines the color of a stochastic sequence. Colors are well-defined for $-1 \le \gamma \le 1$, white for $\gamma = 0$, blue for $\gamma = -1$, and pink for $\gamma = 1$. For $\gamma < -1$ or $\gamma > 1$, colors exist, for example, purple for $\gamma = -2$, red or brown for $\gamma = 2$, and black for $\gamma > 3$. Criteria for color classification are not tight, so a signal with $-1.3 \le \gamma \le -0.5$ can be characterized as bluish, and in the range $0.5 \le \gamma \le 1.5$ as pink or flicker. For time series defined in the time domain, the scaling of their PSD does not exceed the value of 2.[73] Equation 15 is an approximation good only for low frequencies. In practice, eq 15 provides adequate scaling exponents for real-life time series only if the scaling holds true for at least 2 decades in the frequency domain.[59] Spectral methods accurately predict the scaling of synthetic time series produced in the frequency domain, while for those produced in the time domain, half of the spectra estimates deviate significantly for the nominal value of γ.[74] The sign of the exponent characterizes a process as antipersistent, negative (purple, blue), and as persistent, positive (pink, red, and black). Additionally classification is made regarding the stationary or nonstationary nature of the process: fractional Gaussian noises, fGn, (stationary processes) for $-1 < \gamma < 1$, and fractional Brownian motion, fBm, for $1 < \gamma < 3$ (nonstationary process). Notice that fBm is the integration of fGn up to time t. Assuming either fGn or fBm as the kind of the underlying stochastic process, then there is a direct connection between the Hurst exponent and the power spectrum scaling exponent[59]

$$\gamma = \begin{cases} 2H_{RA} - 1 & -1 < \gamma < 1 \\ 2H_{GMM} + 1 & 1 < \gamma < 3 \end{cases} \tag{16}$$

In eq 16, the subscript refers to the analysis method used to obtain the Hurst exponent: RA for stationary noises and GMM for nonstationary. By using the path of analysis described above, one can easily find the scaling exponent describing the viscoelastic properties of the cell, eq 14, as well as the scaling exponent providing information about the noise properties of the cell, eq 16, assuming the existence of fractional Gaussian noises.

MATERIALS AND EXPERIMENTAL PART

We test our model on a rubber that is a "nonliving" material; polydimethylsiloxane (PDMS) has been used as the sample.

https://doi.org/10.1021/acs.jpcb.1c01752
J. Phys. Chem. B 2021, 125, 10883−10892

Two sets of four AFM-NI experiments each have been carried out with the same setup of the experiments carried out in spores and two different control conditions. The first one considers the velocity of penetration, u = 0.029 μm/s, very similar to the velocity of penetration in spores, and the second one considers a much higher velocity of penetration, u = 0.49 μm/s, see below. A detailed analysis of these experiments is given at Section I of the Supporting Information, see also Figures S1a,b, S2, and S3a,b as well as results listed in Table S1. The time derivatives of the measured deflection signals (Figure S1a,b) correspond to nonstationary time series, and analysis has been made by GMM. For the first control condition, GMM delivers viscoelastic exponents in the range [0.758−0.850], for approach, and in the range [0.734−0.758], for retraction. Both phases describe a liquid-like behavior of the "nonliving" material. For the second control condition, the corresponding values are [0.362−0.415] for approach and [0.316−0.342] for retraction, and the "nonliving" material behaves as a viscoelastic one. We found by using two control conditions of substantial difference in the velocity of penetration that the higher the velocity of penetration, the more elastic the material appears.[21] We also used eqs 4 and 6 to fit directly the measured deflection signals for all experiments. Equation 4 fits well the approach phase for both control conditions, returning exponents in very good agreement with what has been obtained by GMM, see Table S1. On the contrary, fittings with eq 6 (retraction) return values of β reduced by at least a factor of 4(2) for 0.029(0.49) μm/s with respect to the approaching phase and to what is obtained by GMM. This inconsistency may be due to additional contributions, for example, drift and/or feedback electronics, which challenge the assumption of a monotonic decreasing contact area, a necessary condition for the application of eq 6. These contributions cannot affect the GMM since the latter uses the absolute changes between two observables.

Living *Ulocladium chartarum* spores were cultivated on potato dextrose agar (Merck, pH = 5.6) at 298 K. A part of the culture was uniformly spread over an area of 250 mm^2 on the coverslip substrate under an optical metallographic microscope (Leica DMRX). The spore cells were left to dry on air after removing traces of humidity with a paper filter. Caution was taken to form monolayers of spores, preventing inner spore shielding. The nanoindentation was carried out with the same type of cantilever under ambient conditions using a phosphorus-(n)-doped silicon cantilever (Bruker RTESPA-300) having a nominal spring constant and a resonance frequency of 40 N/m and 300 kHz, respectively. A stiff cantilever has been chosen to ensure that the tip penetrates inside the hard *Ulocladium chartarum* membrane.[75] This choice may reduce the hysteresis between approach and retraction, see Figure 2.

FDCs were recorded at different points, regularly distributed over preselected areas in the center of the cell, and away from the spore edges, thus avoiding artifacts introduced by cell boundaries. We have conducted 13 experiments, and three constant velocities, namely, 0.0248/0.0289/0.0331 μm/s, have been used. The maximum penetration depth lies in the range of 100−133 nm, but there is also a value of 83 nm as well as of 207 nm.

Figure 2 shows some FDCs in AFM-NI experiments; note that in all experiments we used only one type of cantilever. The deflection signal in volts can be turned into force by multiplying the voltage values by a proper conversion factor, which may also present dependency on the geometry of the laser beam. The treatment is independent on voltages or forces since the beta value involves differences and does not dependent on the conversion factor. The recorded curves consist of 1024 sampling points, and thus, the phase changes from approach to retraction at the time moment t_m, which corresponds to the 512 sampling point. The curves are converted into time units when multiplied by the minimum lag time (reciprocal of the sampling rate), which is approximately equal to 23.6 ms.

RESULTS AND DISCUSSION

The approach and retraction pathways do not coincide, Figure 2. Approach and retraction evolve under constant velocity, which has been kept slow with respect to the timescale of molecular re-organization. The two processes, therefore, form a pair of dynamical processes that do not coincide and evolve near equilibrium. In principle, the response mechanisms governing these processes in living cells can differ and, accordingly, differentiate the response of a biological system under the stimulus of the same mechanical object. Approach and retraction are treated separately for each experiment. To estimate the scaling exponent β, we use the curves depicted in Figure 3a/Figure 3c, which are parts of the overall FDCs and

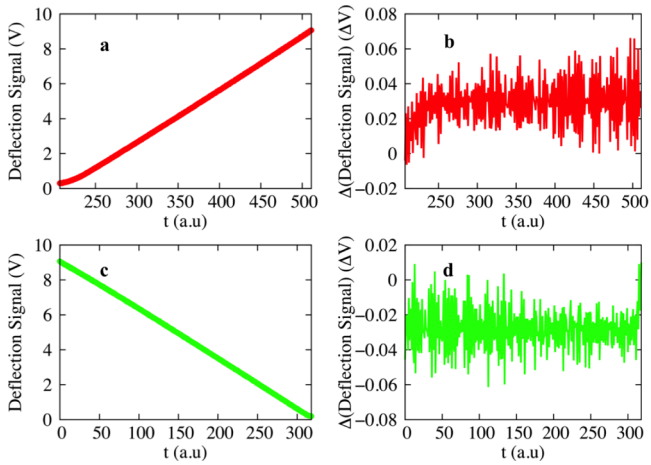

Figure 3. Color code: approach (red) and retraction (green). Recorded deflection signal in a typical AFM-NI experiment is illustrated in (a,c) where data after/before the contact point for approach/retraction are used. The differentiation of the recorded signal is given in (b,d) for approach and retraction, respectively. These data sets are studied by using GMM and RA.

correspond to measurements taken with the tip in contact with the sample. These parts of a FDC form discrete time series of equidistant points, F_i^j, i = 0, 1, 2, .., K, where every pair of two consecutive points is separated by the minimum time lag, τ, and K provides the maximum number of data points of which the analyzed part of the curve is consisted of. The obtained time series are nonstationary, see Figure 3a,c.The index j stands for the phase and takes two values, j = app or j = ret for approach and retraction, respectively.

We apply GMM in order to verify if f_i^j is stationary or not, Figure 3b,d. For all experiments, for both approach and retraction, GMM analysis returns a zero value for H_{GMM}. It implies that f_i^j are stationary and their further analysis is made using RA by means of eq 12. Linear regression of eq 12 returns

https://doi.org/10.1021/acs.jpcb.1c01752
J. Phys. Chem. B 2021, 125, 10883−10892

the values of H_{RA}, eq 13. Figure 4 shows the best fits as well as the estimated exponents for four experiments. The obtained

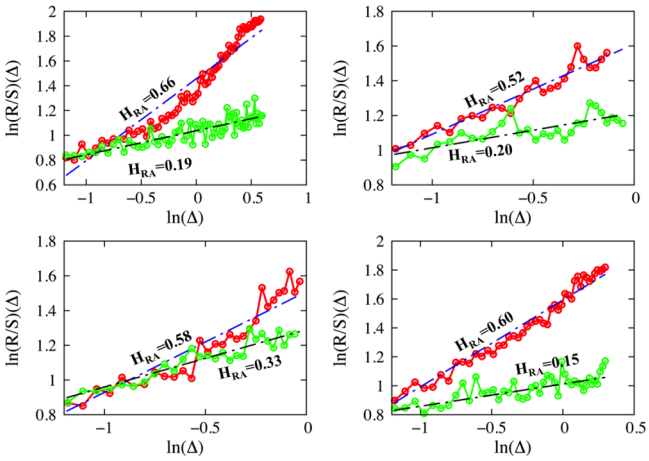

Figure 4. Four different experiments are illustrated. Each panel describes the application of RA for the approach and the retraction phase of the same experiments. Color code: red for approach and green for retraction. Fittings have been performed by using eq 13, dashed blue/black lines for approach and retraction, respectively. The slope of each fit returns the Hurst exponent, H_{RA}, which is also depicted in the graphs.

Hurst exponents, H_{RA}, differentiate pathways for approach and retraction. For the approaching phase and for similar maximum penetration depths of about ∼100 nm (only in one experiment the maximum penetration depth is ∼200 nm), we obtain values of H_{RA} lying in the range $0.48 \leq H_{RA} \leq 0.75$. For the same experiments in the retracting phase, the returned value of H_{RA} lies in the range $0.15 \leq H_{RA} \leq 0.33$, see Table 1.

The scaling exponents characterize the viscoelastic properties of the cell, which are obtained by using eq 14; their values are listed in Table 1; and they are illustrated in Figure 5. In the approaching phase, the Hurst exponents are greater than or equal to 0.48, which is typical either of uncorrelated processes for values close to 0.5 or of slightly persistent processes for larger values. It means that the cell, in most of the cases, attempts to counterbalance nearly perfect the effect of the tip. Additionally, the conjugated scaling exponents, β, eq 14, lie in the range of $0.25 \leq \beta \leq 0.52$. The values align with the literature where β is often found to lie in the range of 0.1−0.3.[26,27] Values of β close to 0.4 have been reported for

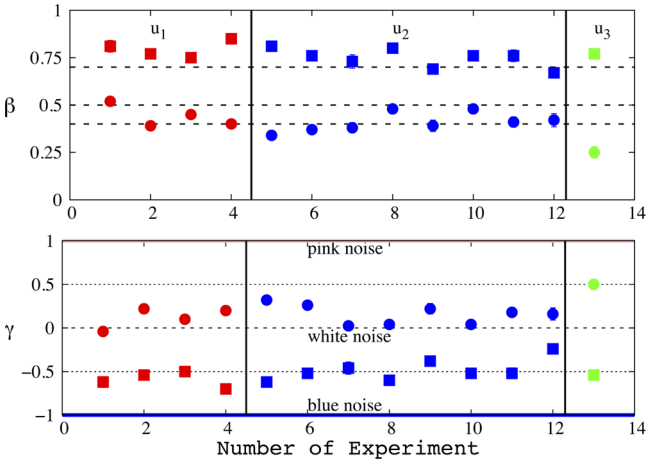

Figure 5. Color code to assist the eye for different constant loads: red for u_1 = 0.0248 μm/s, blue for u_2 = 0.0289 μm/s, and green for u_3 = 0.0331 μm/s. Symbols: circles for the approaching phase and squares for the retracting one. Top: scaling exponents, β, of the viscoelastic properties of cell. Bottom: scaling exponent, γ, of the power spectrum. Three horizontal lines stand for some well-defined colors: blue for $\gamma = -1$, white for $\gamma = 0$, and pink for $\gamma = 1$.

fibroblast (NIH 3T3),[21] and values close to 0.5 have been found for the maximum penetration depth deeper than 1 μm[30] (not reached in the current study). On the other hand, increased values of β and close to 0.5 have been associated with regions of the cell in the periphery of the center. The values of β are somewhat scattered, and they do not depend on the values of the low velocities used here.[21] The exception is the single value for the control condition 0.033 μm/s, which might introduce a dependency condition, and its statistical significance possibly remains to be clarified in future experiments. A comprehensive microscopic interpretation of what the scaling exponent β represents is still missing, albeit that it has been proposed that β represents the turnover dynamics of cytoskeletal proteins and cross-linkers, including myosin motor activity.[26] Cytoskeletal protein dynamics is essential for contraction and locomotion[76] and has been reported to be higher in peripheral areas of the cell such as in the lamella and the lamellipodium, resulting in increased values of β. The scattered values of β, Figure 5, for similar penetration depths likely indicate cell inhomogeneity. It has been reported that there is no evidence for a dependence of the value of β on

Table 1. Approach/Retraction Process for Different Points Regularly Distributed over Preselected Areas in the Center of a *Ulocladium chartarum* Spore[a]

		Approach			retraction		
exp.	u (μm/s)	H_{RA}	β	γ	H_{RA}	β	γ
1, 2	0.0248	0.48 ± 0.025, 0.61 ± 0.014	0.52, 0.39	−0.04, 0.22	0.19 ± 0.031, 0.23 ± 0.015	0.81, 0.77	−0.62, −0.44
3, 4	0.0248	0.55 ± 0.015, 0.60 ± 0.016	0.45, 0.40	0.10, 0.20	0.25 ± 0.018, 0.15 ± 0.016	0.75, 0.85	−0.50, −0.70
5, 6	0.0289	0.66 ± 0.024, 0.63 ± 0.022	0.34, 0.37	0.32, 0.26	0.19 ± 0.013, 0.24 ± 0.024	0.81, 0.76	−0.62, −0.52
7, 8	0.0289	0.62 ± 0.027, 0.52 ± 0.021	0.38, 0.48	0.24, 0.04	0.27 ± 0.035, 0.20 ± 0.024	0.73, 0.80	−0.46, −0.60
9, 10	0.0289	0.61 ± 0.030, 0.52 ± 0.020	0.39, 0.48	0.22, 0.04	0.31 ± 0.026, 0.24 ± 0.026	0.69, 0.76	−0.38, −0.52
11, 12	0.0289	0.59 ± 0.027, 0.58 ± 0.035	0.41, 0.42	0.18, 0.16	0.24 ± 0.031, 0.33 ± 0.017	0.76, 0.67	−0.52, −0.34
13	0.0331	0.75 ± 0.030	0.25	0.50	0.23 ± 0.023	0.77	−0.54

[a]The f_i^j time series created by the raw data are first treated by using GMM. The method delivers $H_{GMM} = 0.0$ for all experiments and for both phases, thus proving the stationary nature of the f_ij. The same time series are then treated by RA, which delivers the scaling exponents, H_{RA}, of the derivative of the response force by means of eq 14, and the standard error of estimate is also provided. By using eqs 14 and 16, we obtain the scaling exponents characterizing the viscoelastic material and the PSD, β and γ, respectively.

https://doi.org/10.1021/acs.jpcb.1c01752
J. Phys. Chem. B 2021, 125, 10883−10892

the depth of penetration,[30] an argument also satisfied in this study for the experiment number 5, where the penetration depth is almost double with respect to the other ones.

The retracting phase of each experiment reveals an entirely different picture. The values of the Hurst exponent lie in the range of $0.15 \leq H_{RA} \leq 0.33$, suggesting an antipersistent process, where each step likely goes in the opposite direction of the previous one. It means that the tip experiences forces that oppose the predefined motion imposed by the tip and are of the same order of the latter. These forces are likely to be of capillary nature, caused by liquid filling of the path created by the tip during the penetration. The liquid nature of the path is corroborated by the values of the scaling exponent β lying in the range $0.67 \leq \beta \leq 0.85$, which is typical of liquid-like materials.[26,27,30] Different responses of approaching retracting AFM-NI curves are associated with biomemory effects of cells for tracing maximum viability lines. External stress is responsible for exuding intracellular substances on the cell wall and a change in the intracellular environment for protecting the cell.[1,2,77−79]

For stationary processes, the value of γ underlines the color of the process. γ can be obtained by using either eq 15 or eq 16. Application of eq 15, which requires a direct transformation of the differentiated data to Fourier space and then fitting with eq 15, presents significant standard error of the estimate, see Section II of the Supporting Information. We obtained the scaling exponents by using eq 16. In the approaching phase, we find $0 < \gamma \leq 0.5$, persistent noises, and accordingly, during this phase, the cell retains a memory. On the other hand, the retracting phase is described by $-0.7 \leq \gamma \leq -0.34$, bluish type of noises, and values describe the antipersistence process again in line with properties underlined by the values of β. Bluish noises have been reported in the literature as noise patterns used by retina cells to yield the visual resolution.[80] For both approach and retraction, the time derivative of the response force is described as the fractional Gaussian noise, obtained values of γ, see Figure 5. This finding is introduced here for the very first time and could be exploited in the modeling of the AFM-NI motion, for instance, in terms of a fractional Langevin-type equation where the proper form of the environmental noise must be chosen. Such a strict mathematical description of the cell response under an AFM indenter of pyramidal shape can provide further information on the microscopic nature of the scaling exponent β. We leave this task for a future work.

CONCLUSIONS

In summary, a robust methodology for the analysis of AFM-NI FDCs is proposed, which can also be extended to incorporate contributions from the solid support. The analysis of experiments conducted in living *Ulocladium chartarum* spores shows that approaching and retracting phases are truly different processes. Their different natures appear (a) by the scaling exponents describing their viscoelastic properties and (b) by the scaling exponents of their PSD, which is connected to the type of the environmental noise. In the approaching phase, the cell presents a viscoelastic behavior similar to what has already been reported in the literature. The process is persistent, underlining a synergic action of the inner components of cell opposing the motion of the tip. The retracting phase corresponds to an antipersistent process and displays characteristics of a liquid-like material, which interacts with the tip by forces that are likely of capillary nature. These forces originate on the release of proteins and biosubstances, triggered by a mechanical stimulus, that fill the path created by the tip and indicate a biomemory response of cells to local mechanical stress as the one imposed by the AFM tip during indentation. The environmental noise is bluish for the retracting phase and persistent, quasi flicker, for the approaching one.

ASSOCIATED CONTENT

Supporting Information

The Supporting Information is available free of charge at https://pubs.acs.org/doi/10.1021/acs.jpcb.1c01752.

Analysis of the deflection signals for two control conditions measured by using a "nonliving" material; recorded deflection signals in AFM-NI versus time; structure function versus the order of the moment; viscoelastic exponents obtained by using eq 14, as well by using eqs 4 and 6; and power spectrum scaling exponents obtained either directly by the linear regression of eq 15 or indirectly by using eq 16 (PDF)

AUTHOR INFORMATION

Corresponding Author

Evangelos Bakalis − *Dipartimento di Chimica "G. Ciamician", Universita di Bologna, Bologna 40126, Italy;* orcid.org/0000-0002-0036-7887; Email: evangelos.bakalis2@unibo.it

Authors

Vassilios Gavriil − *Theoretical and Physical Chemistry Institute, National Hellenic Research Foundation, Athens 11635, Greece*

Alkiviadis-Constantinos Cefalas − *Theoretical and Physical Chemistry Institute, National Hellenic Research Foundation, Athens 11635, Greece*

Zoe Kollia − *Theoretical and Physical Chemistry Institute, National Hellenic Research Foundation, Athens 11635, Greece*

Francesco Zerbetto − *Dipartimento di Chimica "G. Ciamician", Universita di Bologna, Bologna 40126, Italy;* orcid.org/0000-0002-2419-057X

Evangelia Sarantopoulou − *Theoretical and Physical Chemistry Institute, National Hellenic Research Foundation, Athens 11635, Greece*

Complete contact information is available at: https://pubs.acs.org/10.1021/acs.jpcb.1c01752

Notes

The authors declare no competing financial interest.

ACKNOWLEDGMENTS

This work was funded under the frame of the projects "ELI−LASERLAB Europe Synergy, HiPER and IPERION-CH.gr" (MIS 5002735) which is implemented under the Action "Reinforcement of the Research and Innovation Infrastructure", funded by the Operational Programme "Competitiveness, Entrepreneurship and Innovation" (NSRF 2014−2020) and co-financed by Greece and the European Union (European Regional Development Fund) and "Advanced Materials and Devices" (MIS 5002409) which is implemented under the "Action for the Strategic Development on the Research and Technological Sector", funded by the Opera-

tional Programme "Competitiveness, Entrepreneurship and Innovation" (NSRF 2014−2020) and co-financed by Greece and the European Union (European Regional Development Fund).

REFERENCES

(1) Sarantopoulou, E.; Gomoiu, I.; Kollia, Z.; Cefalas, A. C. Interplanetary survival probability of Aspergillus terreus spores under simulated solar vacuum ultraviolet irradiation. *Planet. Space Sci.* **2011**, *59*, 63.
(2) Sarantopoulou, E.; Stefi, A.; Kollia, Z.; Palles, D.; Petrou, P. S.; Bourkoula, A.; Koukouvinos, G.; Velentzas, A. D.; Kakabakos, S.; Cefalas, A. C. Viability of Cladosporium herbarum spores under 157nm laser and vacuum ultraviolet irradiation, low temperature (10K) and vacuum. *J. Appl. Phys.* **2014**, *116*, 104701.
(3) Lautenschläger, F.; Paschke, S.; Schinkinger, S.; Bruel, A.; Beil, M.; Guck, J. The regulatory role of cell mechanics for migration of differentiating myeloid cells. *Proc. Natl. Acad. Sci. U.S.A.* **2009**, *106*, 15696−15701.
(4) Janmay, P. A.; McCulloch, C. A. Cell mechanics: integrating cell responses to mechanical stimuli. *Annu. Rev. Biomed. Eng.* **2007**, *9*, 1−34.
(5) Hoffman, B. D.; Crocker, J. C. Cell mechanics: dissecting the physical response of cells to force. *Annu. Rev. Biomed. Eng.* **2009**, *11*, 259−288.
(6) Fletcher, D. A.; Mullins, R. D. Cell mechanics and the cytoskeleton. *Nature* **2010**, *463*, 485−492.
(7) Pollard, T. D.; Cooper, J. A. Actin, a central player in cell shape and movement. *Science* **2009**, *326*, 1208−1212.
(8) Semashko, V. V.; Pudovkin, M. S.; Cefalas, A.-C.; Zelenikhin, P. V.; Gavriil, V. E.; Nizamutdinov, A. S.; Kollia, Z.; Ferraro, A.; Sarantopoulou, E. Tiny Rare-Earth Fluoride Nanoparticles Activate Tumour Cell Growth via Electrical Polar Interactions. *Nanoscale Res. Lett.* **2018**, *13*, 370.
(9) Cefalas, A.-C.; Gavriil, V.; Ferraro, A.; Kollia, Z.; Sarantopoulou, E. Dynamics and Physics of Integrin Activation in Tumor Cells by Nano-Sized Extracellular Ligands and Electromagnetic Fields. *The Integrin Interactome. Methods in Molecular Biology*; Vicente-Manzanares, M., Ed.; Humana: New York, NY, 2021; Vol. *2217*, p 197.
(10) Suresh, S. Biomechanics and biophysics of cancer cells. *Acta Biomater.* **2007**, *3*, 413−438.
(11) Lanzicher, T.; Martinelli, V.; Puzzi, L.; Del Favero, G.; Codan, B.; Long, C. S.; Mestroni, L.; Taylor, M. R. G.; Sbaizero, O. The cardiomyopathy lamin A/C D192G mutation disrupts whole-cell biomechanics in cardiomyocytes as measured bycatomic force microscopy loading-unloading curve analysis. *Sci. Rep.* **2015**, *5*, 13388.
(12) Otto, O.; et al. Real-time deformability cytometry: on-the-fly cell mechanical phenotyping. *Nat. Methods* **2015**, *12*, 199−202.
(13) Gavara, N. A beginner's guide to atomic force microscopy probing for cell mechanics. *Microsc. Res. Tech.* **2017**, *80*, 75−84.
(14) Moeendarbary, E.; Harris, A. R. Cell mechanics: principles, practices, and prospects. *Wiley Interdiscip. Rev. Syst. Biol. Med.* **2014**, *6*, 371−388.
(15) Wu, P.-H.; et al. A comparison of methods to assess cell mechanical properties. *Nat. Methods* **2018**, *15*, 491−498.
(16) Mahaffy, R. E.; Park, S.; Gerde, E.; Käs, J.; Shih, C. K. Quantitative analysis of the viscoelastic properties of thin regions of fibroblasts using atomic force microscopy. *Biophys. J.* **2004**, *86*, 1777−1793.
(17) Plodinec, M.; et al. The nanomechanical signature of breast cancer. *Nat. Nanotechnol.* **2012**, *7*, 757−765.
(18) Hertz, H. On contact between elastic bodies. *J. Reine Angew. Math* **1882**, *94*, 156−171.
(19) Landau, L. D.; Lifshitz, E. M. *Theory of Elasticity*, 3rd ed.; Butterworth-Heinemann: Oxford, U.K., 1986.
(20) Garcia, P. D.; Garcia, R. Determination of the viscoelastic properties of a single cell cultured on a rigid support by force microscopy. *Nanoscale* **2018**, *10*, 19799.
(21) Garcia, P. D.; Guerrero, C. R.; Garcia, R. Nanorheology of living cells measured by AFM-based force-distance curves. *Nanoscale* **2020**, *12*, 9133.
(22) Desprat, N.; Richert, A.; Simeon, J.; Asnacios, A. Creep function of a single living cell. *Biophys. J.* **2005**, *88*, 2224−2233.
(23) Pullarkat, P.; Fernandez, P.; Ott, A. Rheological properties of the eukaryotic cell cytoskeleton. *Phys. Rep.* **2007**, *449*, 29−53.
(24) Hecht, F. M.; Rheinlaender, J.; Schierbaum, N.; Goldmann, W. H.; Fabry, B.; Schäffer, T. E. Imaging viscoelastic properties of live cells by AFM: Power-law rheology on the nanoscale. *Soft Matter* **2015**, *11*, 4584−4591.
(25) Alcaraz, J.; Buscemi, L.; Grabulosa, M.; Trepat, X.; Fabry, B.; Farré, R.; Daniel, D. Microrheology of human lung epithelial cells measured by atomic force microscopy. *Biophys. J.* **2003**, *84*, 2071−2079.
(26) Kollmannsberger, P.; Fabry, B. Linear and Nonlinear Rheology of Living Cells. *Annu. Rev. Mater. Res.* **2011**, *41*, 75−97.
(27) Rother, J.; Nöding, H.; Mey, I.; Janshoff, A. Atomic force microscopy-based microrheology reveals significant differences in the viscoelastic response between malign and benign cell lines. *Open Biol. J.* **2014**, *4*, 140046.
(28) Fabry, B.; Maksym, G. N.; Butler, J. P.; Glogauer, M.; Navajas, D.; Fredberg, J. J. Scaling the microrheology of living cells. *Phys. Rev. Lett.* **2001**, *87*, 148102.
(29) Christensen, R. M. *Theory of Viscoelasticity*; Academic Press: New York, 1982.
(30) Bruckner, B. R.; Noding, H.; Janshoff, A. Viscoelastic Properties of Confluent MDCK II Cells Obtained from Force Cycle Experiments. *Biophys. J.* **2017**, *112*, 724−735.
(31) Mainardi, F.; Spada, G. Creep, relaxation and viscosity properties for basic fractional models in rheology. *Eur. Phys. J. Spec. Top.* **2011**, *193*, 133−160.
(32) Podlubny, I. *Fractional Differential Equations*; 1st ed.; Academic Press, 1998.
(33) Metzler, R.; Klafter, J. The Random Walk's Guide to Anomalous Diffusion: A Fractional Dynamics Approach. *Phys. Rep.* **2000**, *339*, 1−77.
(34) WestColloquium, B. J. Fractional calculus view of complexity: A tutorial. *Rev. Mod. Phys.* **2014**, *86*, 1169.
(35) Valenti, D.; Tranchina, L.; Brai, M.; Caruso, A.; Spagnolo, B. Environmental metal pollution considered as noise: Effects on the spatial distribution of benthic foraminifera in two coastal marine areas of Sicily (Southern Italy). *Ecol. Model.* **2008**, *213*, 449−462.
(36) Fiasconaro, A.; Valenti, D.; Spagnolo, B. Nonmonotonic behavior of spatiotemporal pattern formation in a noisy Lotka-Voltera system. *Acta Phys. Pol., B* **2004**, *35*, 1491.
(37) Chichigina, O. A.; Dubkov, A. A.; Valenti, D.; Spagnolo, B. Stability in a system subject to noise with regulated periodicity. *Phys. Rev. E: Stat., Nonlinear, Soft Matter Phys.* **2011**, *84*, 021134.
(38) Desprat, N.; Guiroy, A.; Asnacios, A. Microplates-based rheometer for a single living cell. *Rev. Sci. Instrum.* **2006**, *77*, 055111.
(39) Harris, A. R.; Peter, L.; Bellis, J.; Baum, B.; Kabla, A. J.; Charras, G. T. Characterizing the mechanics of cultured cell monolayers. *Proc. Natl. Acad. Sci. U.S.A.* **2012**, *109*, 16449−16454.
(40) Moeendarbary, E.; Valon, L.; Fritzsche, M.; Harris, A. R.; Moulding, D. A.; Thrasher, A. J.; Stride, E.; Mahadevan, L.; Charras, G. T. The cytoplasm of living cells behaves as a poroelastic material. *Nat. Mater.* **2013**, *12*, 253−261.
(41) Efremov, Y. M.; Wang, W.-H.; Hardy, S. D.; Geahlen, R. L.; Raman, A. Measuring nanoscale viscoelastic parameters of cells directly from AFM force-displacement curves. *Sci. Rep.* **2017**, *7*, 1541.
(42) Garcia, R. Nanomechanical mapping of soft materials with the atomic force microscope: methods, theory and applications. *Chem. Soc. Rev.* **2020**, *49*, 5850.
(43) Kolmogorov, A. N. A refinement of previous hypotheses concerning the local structure of turbulence in a viscous

https://doi.org/10.1021/acs.jpcb.1c01752
J. Phys. Chem. B 2021, 125, 10883−10892

incompressible fluid at high Reynolds number. *J. Fluid Mech.* **1962**, *13*, 82−85.
(44) Hansen, L. P. Large Sample Properties of Generalized Method of Moments Estimators. *Econometrica* **1982**, *50*, 1029−1054.
(45) Andersen, K.; Castiglione, P.; Mazzino, A.; Vulpiani, A. Simple stochastic models showing strong anomalous diffusion. *Eur. Phys. J. B* **2000**, *18*, 447−452.
(46) Peng, C. K.; Buldyrev, S. V.; Havlin, S.; Simons, M.; Stanley, H. E.; Goldberger, A. L. Mosaic organization of DNA nucleotides. *Phys. Rev. E: Stat., Nonlinear, Soft Matter Phys.* **1994**, *49*, 1685−1689.
(47) Kantelhardt, J. W.; Zschiegner, S. A.; Koscielny-Bunde, E.; Havlin, S.; Bunde, A.; Stanley, H. E. Multifractal detrended fluctuation analysis of nonstationary time series. *Physica A* **2002**, *316*, 87−114.
(48) Scafetta, N.; Grigolini, P. Scaling detection in time series: Diffusion entropy analysis. *Phys. Rev. E: Stat., Nonlinear, Soft Matter Phys.* **2002**, *66*, 036130.
(49) Barunik, J.; Kristoufek, L. On Hurst exponent estimation under heavy-tailed distributions. *Physica A* **2010**, *389*, 3844−3855.
(50) Bakalis, E.; Mertzimekis, T. J.; Nomikou, P.; Zerbetto, F. Breathing modes of Kolumbo submarine volcano (Santorini, Greece). *Sci. Rep.* **2017**, *7*, 46515.
(51) Bakalis, E.; Höfinger, S.; Venturini, A.; Zerbetto, F. Crossover of two power laws in the anomalous diffusion of a two lipid membrane. *J. Chem. Phys.* **2015**, *142*, 215102.
(52) Sändig, N.; Bakalis, E.; Zerbetto, F. Stochastic analysis of movements on surfaces: The case of C60 on Au(1 1 1). *Chem. Phys. Lett.* **2015**, *633*, 163−168.
(53) Parent, L. R.; Bakalis, E.; Ramirez-Hernandez, A.; Kammeyer, J. K.; Park, C.; de Pablo, J.; Zerbetto, F.; Patterson, J. P.; Gianneschi, N. C. Directly Observing Micelle Fusion and Growth in Solution by Liquid-Cell Transmission Electron Microscopy. *J. Am. Chem. Soc.* **2017**, *139*, 17140−17151.
(54) Parent, L. R.; Bakalis, E.; Proetto, M.; Li, Y.; Park, C.; Zerbetto, F.; Gianneschi, N. C. Tackling the Challenges of Dynamic Experiments Using Liquid-Cell Transmission Electron Microscopy. *Acc. Chem. Res.* **2018**, *51*, 3−11.
(55) Bakalis, E.; Parent, L. R.; Vratsanos, M.; Park, C.; Gianneschi, N. C.; Zerbetto, F. Complex Nanoparticle Diffusional Motion in Liquid Cell Transmission Electron Microscopy. *J. Phys. Chem. C* **2020**, *124*, 14881−14890.
(56) Hurst, H. E. Long-term storage capacity of reservoirs. *Trans. Am. Soc. Civ. Eng.* **1951**, *116*, 770−799.
(57) Mandelbrot, B. B.; Wallis, J. R. Robustness of the Rescaled Range R/S in the Measurement of Noncyclic Long Run Statistical Dependency. *Water Resour. Res.* **1969**, *5*, 967.
(58) He, L.-Y.; Qian, W.-B. A Monte Carlo simulation to the performance of the R/S and V/S methods-Statistical revisit and real world application. *Physica A* **2012**, *391*, 3770−3782.
(59) Eke, A.; Herman, P.; Bassingthwaighte, J.; Raymond, G.; Percival, D.; Cannon, M.; Balla, I.; Ikrényi, C. Physiological time series: distinguishing fractal noises from motions. *Pflugers Arch.* **2000**, *439*, 403−415.
(60) Lee, E. H.; Radok, J. R. M. The Contact Problem for Viscoelastic Bodies. *J. Appl. Mech.* **1960**, *27*, 438−444.
(61) Popov, V. L. *Contact Mechanics and Friction, Physical properties and Applications*; Springer: Berlin, Heidelberg, 2010.
(62) Sneddon, I. N. The relation between load and penetration in the axisymmetric Boussinesq problem for a punch of arbitrary profile. *Int. J. Eng. Sci.* **1965**, *3*, 47−57.
(63) Bilodeau, G. G. Regular pyramid punch problem. *J. Appl. Mech.* **1992**, *59*, 519−523.
(64) Ting, T. C. T. Contact stresses between a rigid indenter and a viscoelastic half-space. *J. Appl. Mech.* **1966**, *33*, 845.
(65) Ting, T. C. T. Contact Problems in the Linear Theory of Viscoelasticity. *J. Appl. Mech.* **1968**, *35*, 248−254.
(66) Garcia, P. D.; Garcia, R. Determination of the Elastic Moduli of a Single Cell Cultured on a Rigid Support by Force Microscopy. *Biophys. J.* **2018**, *114*, 2923−2932.
(67) Bakalis, E.; Mertzimekis, T. J.; Nomikou, P.; Zerbetto, F. Temperature and Conductivity as Indicators of the Morphology and Activity of a Submarine Volcano: Avyssos (Nisyros) in the South Aegean Sea, Greece. *Geosciences* **2017**, *8*, 193.
(68) Aranson, I. S.; Rabinovich, M. I.; Tsimring, L. S. Anomalous diffusion of particles in regular fields. *Phys. Lett. A* **1990**, *151*, 523.
(69) Castiglione, P.; Mazzino, A.; Muratore-Ginanneschi, P.; Vulpiani, A. On strong anomalous diffusion. *Physica D* **1999**, *134*, 75−93.
(70) Barabasi, A. L.; Vicsek, T. Multifractality of self-affine fractals. *Phys. Rev. A* **1991**, *44*, 2730−2733.
(71) Ferrari, R.; Manfroi, A. J.; Young, W. R. Strongly and weakly self-similar diffusion. *Physica D* **2001**, *154*, 111−137.
(72) Peters, E. E. *Fractal Market Analysis-Applying Chaos Theory to Investment and Analysis*; 3rd ed.; John Wiley & Sons, Inc.: New York, 1994.
(73) Krapf, D.; Lukat, N.; Marinari, E.; Metzler, R.; Oshanin, G.; Selhuber-Unkel, C.; Squarcini, A.; Stadler, L.; Weiss, M.; Xu, X. Spectral Content of a Single Non-Brownian Trajectory. *Phys. Rev. X* **2019**, *9*, 011019.
(74) Fougere, P. F. On the Accuracy of Spectrum Analysis of Red Noise Processes Using Maximum Entropy and Periodogram Methods: Simulation Studies and Application to Geophysical Data. *J. Geophys. Res.* **1985**, *90*, 4355.
(75) Zhao, L.; Schaefer, D.; Marten, M. R. Assessment of Elasticity and Topography of Aspergillus nidulans Spores via Atomic Force Microscopy. *Appl. Environ. Microbiol.* **2005**, *71*, 955−960.
(76) Lauffenburger, D. A.; Horwitz, A. F. Cell migration: a physically integrated molecular process. *Cell* **1996**, *84*, 359−369.
(77) Beauvais, A.; Latge, J.-P. Special Issue: Fungal Cell Wall. *J. Fungi* **2018**, *4*, 91.
(78) Ouedraogo, J. P.; Hagen, S.; Spielvogel, A.; Engelhardt, S.; Meyer, V. Survival Strategies of Yeast and Filamentous Fungi against the Antifungal Protein AFP. *J. Biol. Chem.* **2011**, *286*, 13859−13868.
(79) Brown, A. J. P.; Cowen, L. E.; di Pietro, A.; Quinn, J. Stress Adaptation. *Microbiol. Spectr.* **2017**, *5*, 1−23.
(80) Yellot, J. I., Jr. Spectral consequences of photoreceptor sampling in the rhesus retina. *Science* **1983**, *221*, 382−385.

https://doi.org/10.1021/acs.jpcb.1c01752
J. Phys. Chem. B 2021, 125, 10883−10892